Springer Ser Chem Sens Biosens (2007) 5: 151–170
DOI 10.1007/5346_026

Published online: 29 July 2006

Studies of Contact Mechanics with the QCM

Diethelm Johannsmann

Institute of Physical Chemistry, Clausthal University of Technology,
Arnold-Sommerfeld-Str. 4, 38678 Clausthal-Zellerfeld, Germany
johannsmann@pc.tu-clausthal.de

Abstract The quartz crystal microbalance can serve as high-frequency probe of the microcontacts formed between the crystal surface and a solid object touching it. On a simplistic level, the load can be approximated by an assembly of point masses, springs, and dashpots. The Sauerbrey model, leading to a decrease in frequency, is recovered if small particles are rigidly attached to the crystal. In another limiting case, the particles are so heavy that inertia holds them in place in the laboratory frame. The spheres exert a restoring force onto the crystal, thereby increasing the stiffness of the composite resonator. The resonance frequency increases in proportion to the lateral spring constant of the sphere–plate contacts. A third limiting case is represented by particles attached to the crystal via a dashpot. Within this model (extensively used in nanotribology) the dashpot increases the bandwidth. The momentum relaxation time τ_S ("slip time") is calculated from the ratio of the increase in bandwidth and the decrease in frequency, $\Delta\Gamma/(-\Delta f)$.

The force–displacement relations in contact mechanics are often nonlinear. A prominent example is the transition from stick to slip. Even for nonlinear interactions, there is a strictly quantitative relationship between the shifts of frequency and bandwidth, Δf and $\Delta\Gamma$, on the one hand, and the force acting on the crystal, $F(t)$, on the other. Δf and $\Delta\Gamma$ are proportional to the in-phase and the out-of-phase component of $F(t)$, respectively. Evidently, $F(t)$ cannot be explicitly derived from Δf and $\Delta\Gamma$. Still, any contact-mechanical model (like the Mindlin model of partial slip) can be tested by comparing the predicted

and the measured values of Δf and $\Delta \Gamma$. Further experimental constraints stem from the measurement of the amplitude dependence of the resonance parameters.

Contacts mechanics in the MHz range is much different from its low-frequency counterpart. For instance, static friction coefficients probed with MHz excitation are often much above 1. Contact mechanics at short time scales should be of substantial practical relevance.

Keywords Contact mechanics · Contact stiffness · Fretting wear · Mindlin model · Nonlinear mechanics · Quartz crystal resonator · Quartz crystal microbalance · Partial slip · Stick-slip

1 Introduction

Contact mechanics is both an old and a modern field. Its classical domains of application are adhesion, friction, and fracture. Clearly, the relevance of the field for technical devices is enormous. Systematic strategies to control friction and adhesion between solid surfaces have been known since the stone age [1]. In modern times, the ground for systematic studies was laid in 1881 by Hertz in his seminal paper on the contact between solid elastic bodies [2]. Hertz considers a sphere–plate contact. Solving the equations of continuum elasticity, he finds that the vertical force, $F_\perp$, is proportional to $\delta^{3/2}$, where δ is the indentation. The sphere–plate contact forms a nonlinear spring with a differential spring constant $\kappa = \mathrm{d}F/\mathrm{d}\delta \propto \delta^{1/2}$. The nonlinearity occurs because there is a concentration of stress at the point of contact. Such stress concentrations – and the ensuing mechanical nonlinearities – are typical of contact mechanics.

Clean, dry single-asperity contacts have intensely been studied both theoretically [3–5] and experimentally [6]. The development of the atomic force microscope (AFM) [7–9] and the surface forces apparatus (SFA) [10–12] have certainly been influential. Both instruments allow for experiments under a control of geometry on the molecular level. Multi-asperity contacts evidently are more difficult to study than clean sphere–plate contacts [13, 14], but are much closer to the real world, as well. Currently, there is quite some activity carrying the knowledge gained on single-asperity contacts to the field of dry and wet granular media [15, 16]. The mechanics of a sand pile (such as its critical angle of sliding, its compactification with time or pressure, or its strengthening upon exposure to water vapor) all depend on the forces (normal and lateral) exerted at the contacts between the individual grains.

Given that nonlinearities are ubiquitous, testing with oscillatory excitation is of less practical importance in contact mechanics than in other fields of material science. For instance, stick-slip motion is most easily studied by steadily pulling the object of interest across the supporting substrate. Oscillatory testing will result in complicated trajectories [17]. Sinusoidal excitation mostly

makes sense in the small-amplitude limit, where force and displacement are linearly (or almost linearly) related. In the linear domain, superposition holds and a system's response is fully specified by its complex, frequency-dependent stiffness. Small nonlinearities can be dealt with in the frame of the two-timing approximation (cf. Sect. 3). Linear behavior, generally speaking, is *always* found in the limit of small stress [5]. This is true for both elastic interactions and sliding. A sliding motion, where the speed is proportional to the force, is termed "creep" in the context of rheology. Linear creep occurs whenever the external force is comparable in magnitude to the random forces related to Brownian motion. The external force then only adds a small bias to the random movement of the sample, and this bias is proportional to the force.

The use of the QCM for contact mechanics has been pioneered by Dybwad [18]. Dybwad placed a sphere onto a quartz resonator and found an *increase* in frequency. He explains this increase by the fact that the sphere rests in place in the laboratory frame due to inertia. It exerts a restoring force onto the crystal, thereby increasing its resonance frequency. He points out that the frequency shift can be exploited to measure the strength of the contact between the sphere and the quartz plate.

Nanotribology has also gained much from the QCM, where the early work has been done by J. Krim [19, 20]. The Krim group studied adsorbed monolayers of noble gas atoms onto the electrode and observed an increase in dissipation. Describing these experiments in the frame of continuum models, where the monolayer would correspond to a film with a viscosity η (Eq. 71 in Chap. 2 of this volume, replace Z_f by $(i\omega\rho\eta)^{1/2}$), cannot explain these findings. The viscosity would have to be orders of magnitude smaller than the viscosity of the corresponding bulk liquid, and it is hard to see why this should be the case. The Krim group models the atoms as discrete objects sliding across the surface. The motion of the atom is coupled to the motion of the surface via a dashpot with a drag coefficient ξ_S. The ratio of mass and drag coefficient has the dimension of a time, called "slip time", τ_S. τ_S is a momentum relaxation time. When the motion of substrate stops abruptly, the speed of the sphere exponentially slows down with a decay time τ_S. There is now experimental evidence that this kind of sliding – at least in certain cases – is not a creep in the sense of biased diffusion. Mistura and coworkers determined the amplitude dependence of the slip time and found a critical minimum amplitude, below which the molecules slick [21]. This finding contradicts liquid-like sliding. In liquid-like sliding, the slip time would be independent of amplitude.

2 Modeling with Discrete Mechanical Elements

In contact mechanics experiments with the QCM, the sample usually does not consist of a planar layer system, but rather of one or more discrete ob-

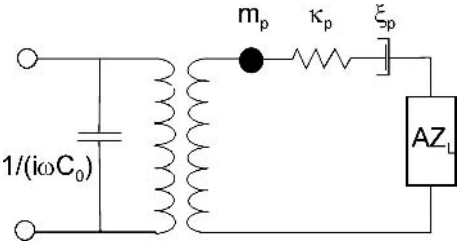

Fig. 1 Equivalent circuit representation of the quartz crystal including a load. Piezoelectric stiffening (described by the element $4Z_k$ in Fig. 13, Chap. 2 in this volume) was neglected. The sample is represented by the load Z_L

jects touching the crystal surface. One can – on a purely heuristic level – describe the sample by an equivalent mechanical model containing elements like a mass, a spring, or a dashpot. The effect, which these elements have on the frequency shift, is readily calculated starting from the small-load approximation (Eq. 51 in Chap. 2 in this volume). We assume that the stress–speed ratio may be replaced by an average stress–speed ratio, where the average stress is just the lateral force divided by the active area of the crystal. Replacing the stress by an average stress certainly is an approximation[1]. It can to some extent be justified by an argument based on the scattering of acoustic waves [22]. Once one has accepted this simple picture, the change of resonance frequency can be easily predicted by means of the Butterworth–van Dyke (BvD) equivalent circuit (Sect. 6 in Chap. 2 in this volume). In the following, we use the version of the BvD circuit, where electrical and mechanical elements are separated as shown in Fig. 1.

2.1 Loading with a Mass

Consider a small sphere rigidly attached to the crystal (Fig. 2). Let the mass of the sphere be m_S. Figure 2a shows a single sphere. Real crystals might be in contact with many such spheres, which is accounted for by including the number density of these spheres, N_S/A, as a prefactor into the equations below. N_S is the number of spheres and A is the active area of the crystal.

If the spheres are small enough, they can be treated like a Sauerbrey film with an areal mass density $m_f = N_S m_S/A$. Let κ_p be the spring constant of the crystal in the BvD sense, m_p the equivalent mass of the crystal in BvD sense (Eq. 116 in Chap. 2 in this volume), and m_q the areal mass density of the

[1] For instance, energy trapping may be affected by a load applied at the center of the disk.

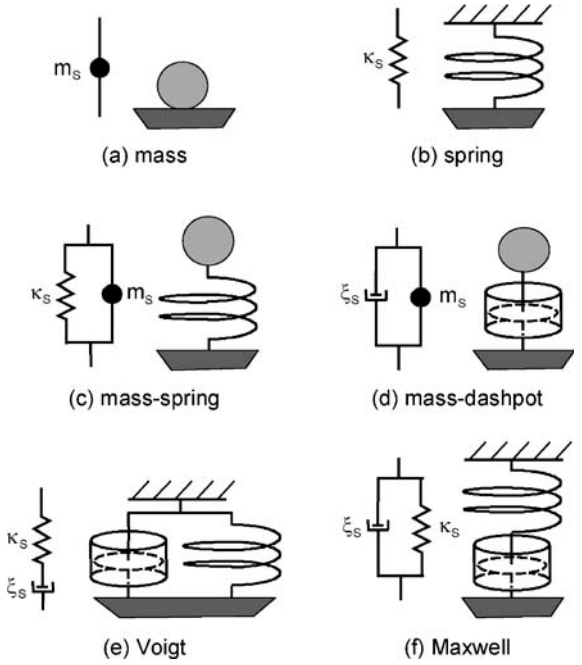

Fig. 2 Different circuits to be inserted for the load in Fig. 1. The conversion from the physical situation (*right*) to the equivalent circuits (*left*) entails a complication because networks are depicted such that the *electrical* Kirchhoff rules apply. Elements which are placed in series, physically, are represented as parallel circuit elements and vice versa (cf. Fig. 5 in Chap. 2 in this volume). For instance, the forces exerted by the spring and the dashpot in *e* are additive. In order to let the corresponding voltages in the electrical circuit also be additive, the circuit elements have to be placed in series. In the literature on polymer rheology, networks of springs and dashpots are drawn according to the physical situation (*right-hand-side* in this figure), which comes down to a different set of Kirchhoff rules

crystal. The frequency shift of the composite resonator then is:

$$\begin{aligned}\Delta f = f_r - f_0 &= \frac{1}{2\pi}\left(\sqrt{\frac{\kappa_p}{m_p + \left(N_S/A\right) m_S}} - \sqrt{\frac{\kappa_p}{m_p}}\right) \\ &= \frac{1}{2\pi}\sqrt{\frac{\kappa_p}{m_p}}\sqrt{\frac{1}{1 + \frac{\left(N_S/A\right) m_S}{m_p}}} - \sqrt{\frac{\kappa_p}{m_p}} \\ &\approx \frac{1}{2\pi}\omega_0\left(1 - \frac{1}{2}\frac{\left(N_S/A\right) m_S}{m_p} - 1\right) = -f_0\frac{m_f}{m_q}, \end{aligned} \tag{1}$$

where f_r is the resonant frequency, f_0 is the resonant frequency of the bare crystal, and $\omega_0 = (\kappa_p/m_p)^{1/2}$ is the radial resonant frequency of the bare crystal. The relation $m_p = Am_q/2$ (Eq. 116 in Chap. 2 in this volume) was used. Equation 1 reproduces the Sauerbrey equation (Eq. 28 in Chap. 2).

The same result is found by use of the small-load approximation (cf. Eq. 51 in Chap. 2) Using the stress $\sigma = -\omega^2(N_S/A)m_S a = -\omega^2 m_f a$ (a is the amplitude of motion) and the speed $\dot{u} = i\omega a \exp(i\omega t)$, one finds:

$$\frac{\Delta f}{f_f} = \frac{i}{\pi Z_q}\frac{\sigma}{\dot{u}} = \frac{i}{\pi Z_q} Z_L = \frac{i}{\pi Z_q}\frac{-\omega^2 m_f a \exp(i\omega t)}{i\omega a \exp(i\omega t)} = \frac{-\omega m_f}{\pi Z_q} = -n\frac{m_f}{m_q}, \qquad (2)$$

where the relation $m_q = Z_q/(2 f_f)$ has been used (Eq. 26 in Chap. 2). $Z_L = \sigma/\dot{u}$ is the load impedance.

2.2 Loading with a Spring

In analogy to Eq. 1, one can add a spring (with a spring constant κ_S) into the BvD circuit, rather than a mass (Fig. 2b). Such a spring would represent the stiffness of a contact between the crystal and an object touching it. The object would have to be so heavy that it does not take part in the movement of the crystal. The analog of Eq. 1 is:

$$\Delta f = f_r - f_0 = \frac{1}{2\pi}\left(\sqrt{\frac{\kappa_p + (N_S/A)\kappa_S}{m_p}} - \sqrt{\frac{\kappa_p}{m_p}}\right)$$
$$\approx f_0\left(1 + \frac{1}{2}\frac{N_S}{A}\frac{\kappa_S}{\kappa_p} - 1\right) = f_f\frac{N_S}{A}\frac{1}{\pi Z_q}\frac{\kappa_S}{\omega}, \qquad (3)$$

where the relation $(\kappa_p m_p)^{1/2} = \kappa_p/\omega_0 \approx \kappa_p/\omega \approx AZ_q n\pi/2$ (Eq. 115 in Chap. 2) has been used. In this context the resonance frequency of the unloaded crystal, ω_0, and the loaded crystal, ω, can be considered to be about equal. The same result is found by application of the small-load approximation if one assumes that the average stress is given by the spring constant multiplied the number density, N_S/A [23]:

$$\frac{\Delta f}{f_f} = \frac{i}{\pi Z_q}\frac{\sigma}{\dot{u}} = \frac{i}{\pi Z_q}\frac{N_S}{A}\frac{\kappa_S u_0}{i\omega u_0} = \frac{i}{\pi Z_q}\frac{N_S}{A}\frac{\kappa_S}{\omega}. \qquad (4)$$

In the following, the small-load approximation is always used to calculate the frequency shift.

The frequency shift in Eq. 4 is *positive*. If the spring constant is independent of frequency, Δf scales as ω^{-1}, that is, as the inverse overtone order, n^{-1}. Damping and frequency dependent interactions can be introduced into Eq. 4

by replacing κ_S with a complex spring constant $\kappa_S(\omega) + i\omega\xi_S(\omega)$, leading to:

$$\frac{\Delta\tilde{f}}{f_f} = \frac{N_S}{\pi Z A_q}\frac{1}{\omega}\left(\kappa_S(\omega) + i\omega\xi_S(\omega)\right) . \tag{5}$$

The parameter $\Delta\tilde{f} = \Delta f + i\Delta\Gamma$ is a complex resonance frequency. Γ is the half-band-half-width (cf. Sect. 2 in Chap. 2 in this volume). The drag coefficient may describe interfacial drag, but also the withdrawal of energy from the crystal via radiation of sound. Equation 5 can be inverted, leading to explicit formulas for $\kappa_S(\omega)$ and $\xi_S(\omega)$:

$$\kappa_S(\omega) = 2\pi^2 Z_q n \frac{A}{N_S}\Delta f(\omega) \tag{6}$$

$$\xi_S(\omega) = \frac{\pi Z_q}{f_f}\frac{A}{N_S}\Delta\Gamma(\omega) . \tag{7}$$

In order to emphasize the generality of the model, the frequency dependence of $\kappa_S(\omega)$ and $\xi_S(\omega)$ was explicitly included in Eqs. 5, 6, and 7. More detailed models (cf. Sects. 2.4 and 2.5) predict the frequency dependence of $\kappa_S(\omega)$ and $\xi_S(\omega)$. For the time being, no such statement is made. The only assumption made here is the absence of inertial effects: Clearly, some of the material close to the contact must move with the crystal. The total mass of this co-moving material was neglected.

2.3 Loading with a Mass in Series with a Spring

In the simple-spring model, the crystal is in contact with an immobile object. The model can be extended to cover situations where the object takes part in the oscillation to some extent. A typical object of this kind would be a small (< 10 μm) sphere [40]. Figure 2c depicts the physical situation and the equivalent circuit representation. Note that the motion occurs into the *lateral* direction even though the spring is drawn vertically. In the following, we assume a spring constant independent of frequency, labeled $\bar{\kappa}_S$. From Fig. 2c, we infer the load to be:

$$\begin{aligned} Z_L &= \frac{N_S}{A}\left({Z_{mass}}^{-1} + {Z_{spring}}^{-1}\right)^{-1} = \frac{N_S}{A}\left(\frac{1}{i\omega m_S} + \frac{i\omega}{\bar{\kappa}_S}\right)^{-1} \\ &= \frac{N_S}{A}\frac{i\omega m_S\bar{\kappa}_S}{-\omega^2 m_S + \bar{\kappa}_S} = \frac{N_S}{A} i\omega m_S \frac{1}{1 - \frac{\omega^2}{\omega_S^2}} , \end{aligned} \tag{8}$$

where the parameter $\omega_S = (\bar{\kappa}_S/m_S)^{1/2}$ denotes the resonance frequency of the mass-spring system. Using the small-load approximation, we find:

$$\frac{\Delta f}{f_f} = \frac{i}{\pi Z_q} Z_L = -\frac{N_S}{A}\frac{\omega m_S}{\pi Z_q}\frac{1}{1-\frac{\omega^2}{\omega_S^2}}. \tag{9}$$

Since the spring constant is complex due to dissipalion, the denominator never becomes zero. Equation 9 was first proposed by Dybwad [19]. In the limits of $\omega_S^2 \gg \omega$ and $\omega_S^2 \ll \omega$, Eq. 9 reproduces the Sauerbrey equation (Eq. 2) and the simple-spring model (Eq. 4), respectively. Equation 9 can also be derived from Eq. 91 in Chap. 2 in this volume by expanding all tangents to first order. This amounts to a continuum model of the same experimental situation, where the contacts and the spheres correspond to a "soft", first layer and a "hard", second layer, respectively.

2.4 Loading with a Mass in Series with a Dashpot

The connection between the sphere and the crystal can also be made across a dashpot (Fig. 2d). This model is extensively used for the interpretation of nanotribological experiments with the QCM [20]. We consider the drag coefficient of the dashpot, $\bar{\xi}_S$, to be a fixed parameter independent of frequency. Within this model, the sphere slides on the surface in a liquid-like sense (creep). This liquid-like friction is very different from interfacial sliding in the Coulomb sense. For Coulomb sliding, the friction force is proportional to the vertical load with a dimensionless dynamic friction coefficient, μ_D. In particular, the friction force is independent of the sliding speed. Sliding in the Coulomb sense implies a strongly nonlinear force–speed relation. The drag force in creep, on the other hand, depends linearly on sliding speed.

From Fig. 2d one reads:

$$\begin{aligned} Z_L &= \frac{N_S}{A}\left(Z_{\text{mass}}{}^{-1} + Z_{\text{dashpot}}{}^{-1}\right)^{-1} = \frac{N_S}{A}\left(\frac{1}{i\omega m_S} + \frac{1}{\bar{\xi}_S}\right)^{-1} \\ &= \frac{N_S}{A}\frac{i\omega m_S \bar{\xi}_S}{i\omega m_S + \bar{\xi}_S} = \frac{N_S}{A} i\omega m_S \frac{1}{1+i\omega\tau_S} = \frac{N_S}{A} i\omega m_S \frac{1-i\omega\tau_S}{1+i\omega^2\tau_S^2}, \end{aligned} \tag{10}$$

where the slip time $\tau_S = m_S/\bar{\xi}_S$ was used. Using the small-load approximation, we find [19, 24]:

$$\frac{\Delta\tilde{f}}{f_f} = -\frac{N_S}{A\pi Z_q}\omega m_S \frac{1-i\omega\tau_S}{1+\omega^2\tau_S^2}. \tag{11}$$

The tilde denotes a complex frequency shift. We write $\Delta\tilde{f} = \Delta f + i\Delta\Gamma$. The imaginary part, $\Delta\Gamma$, is the shift of the half bandwidth at half maximum. The

slip time is inferred from the ratio of $\Delta\Gamma$ and $(-\Delta f)$ as:

$$\tau_S = \frac{1}{\omega}\frac{\Delta\Gamma}{(-\Delta f)}\,. \tag{12}$$

The mass-dashpot model predicts that the ratio $\Delta\Gamma/(-\Delta f)$ scales as the overtone order (unless the slip time itself depends on frequency).

2.5 Loading with a Spring and a Dashpot

The extension of the previous models to a sphere coupled to the plate via a spring and a dashpot is straightforward. The coupling can be achieved either via a Voigt-type circuit (viscoelastic solid, Fig. 2e) or via a Maxwell-type circuit (viscoelastic liquid, Fig. 2f). Below, we assume that the object is so heavy that it does not take part in the motion. When the mass is infinite, the inertial term drops out of the load impedance. An infinite mass is graphically depicted as a wall. For Voigt-type coupling we find:

$$Z_L = \frac{N_S}{A}\left(Z_{\text{spring}} + Z_{\text{dashpot}}\right) \approx \frac{N_S}{A}\left(\frac{\bar{\kappa}_S}{i\omega} + \bar{\xi}_S\right) \tag{13}$$

leading to a frequency shift of:

$$\frac{\Delta\tilde{f}}{f_f} = \frac{1}{\pi Z_q}\frac{N_S}{A\omega}\left(\bar{\kappa}_S + i\omega\bar{\xi}_S\right). \tag{14}$$

Voigt-type coupling makes sense for multi-asperity contacts. The load-bearing asperities correspond to springs, but there will also be interfacial drag (for instance across capillary bridges) acting in parallel to the elastic contacts. The model predicts a positive frequency shift, which scales as the inversely overtone order, n^{-1}. Both the positive frequency shift and the n^{-1}-scaling are rather characteristic experimental features. Checking for the n^{-1}-scaling, one can easily determine whether or not Voigt-type coupling applies.

Figure 3 shows an example [25]. A monolayer of glass spheres with a diameter of 200 μm was deposited onto the crystal at $t = 0$ (state I). The initial deposition had virtually no effect on the frequency of resonance. Even though the spheres did touch the crystal, the dry contacts only transmitted a minute amount of stress. After about 10 min, the chamber was filled with saturated water vapor, leading to a substantial frequency increase (state II). Capillary forces strengthen the contacts, as known from the sand-castle effect. A further strong increase in frequency was achieved by ramping the humidity back down to a low value (state III). After having been exposed to water vapor, the spheres form a cake. The latter transition is reversible: once the assembly of spheres has been soaked in humid air, one can go back and forth between the states II and III. Comparing the frequency shifts on the different

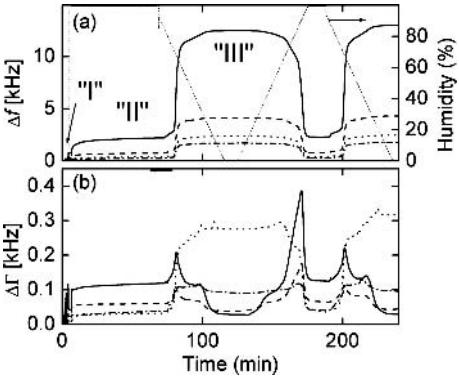

Fig. 3 Shifts of frequency (**a**) and bandwidth (**b**) experienced by a quartz crystal covered with a monolayer of glass spheres (diameter $d = 200\,\mu m$) exposed to humid air. *States I, II*, and *III* correspond to the initial state right after deposition, to humid air, and to a dry state reached after soaking the sample in humid air for a while and then returning to the dry state, respectively. *Full line* 5 MHz, *dashed line* 15 MHz, *dotted line* 25 MHz, *dash-dotted line* 35 MHz (adapted from [28])

overtones, one confirms n^{-1} scaling. This experiment proves the QCM to be a non-destructive monitoring device for capillary aging [26].

For Maxwell-type coupling, the situation is more complicated. From Fig. 2f, one reads:

$$Z_L \approx \frac{N_S}{A}\left(Z_{spring}{}^{-1} + Z_{dashpot}{}^{-1}\right)^{-1} = \frac{N_S}{A}\left(\frac{i\omega}{\bar{\kappa}_S} + \frac{1}{\bar{\xi}_S}\right)^{-1}$$

$$= \frac{N_S}{A}\frac{\bar{\kappa}_S\bar{\xi}_S}{\bar{\kappa}_S + i\omega\bar{\xi}_S} = \frac{N_S}{A}\bar{\xi}_S\frac{1}{1 + i\omega\tau_R} = \frac{N_S}{A}\bar{\xi}_S\frac{1 - i\omega\tau_R}{1 + i\omega^2\tau_R^2}. \tag{15}$$

A retardation time $\tau_R = \bar{\xi}_S/\bar{\kappa}_S$ was introduced. For the frequency shift, we find:

$$\frac{\Delta\tilde{f}}{f_f} = \frac{N_S}{A}\frac{i}{\pi Z_q}\bar{\xi}_S\frac{1 - i\omega\tau_R}{1 + i\omega^2\tau_R^2} = \frac{N_S\bar{\xi}_S}{A\pi Z_q}\frac{\omega\tau_R + i}{1 + \omega^2\tau_R^2}. \tag{16}$$

The frequency shift is positive. The n-scaling depends on the value of $\omega\tau_R$. In the limit of $\omega\tau_R \gg 1$, n^{-1} scaling is found. In this case, the relaxation time is much longer than the period of oscillation and the Maxwell element behaves elastically. The Maxwell model reduces to the simple-spring model (Sect. 2.2). If, on the other hand, the retardation time is short ($\omega\tau_R \ll 1$), the frequency shift is still positive, but it scales linearly with n. If a positive frequency shift in conjunction with linear n-scaling is found, this in indicative of fast relaxation processes in the contact zone. If this is the case, the damping must also be large.

Two caveats are worth mentioning: Firstly, inertial effects can only be neglected if the contact area is small enough. Otherwise, the co-moving mass needs to be included into the model. The co-moving volume is much smaller than the volume of the entire sphere but it may be nonzero. Secondly, there usually is some increase in bandwidth originating from the radiation of acoustic waves into the sphere. Acoustic radiation can be accounted for by adding a dashpot with a drag coefficient ξ_{ac} as a parallel element into the circuits shown in Fig. 2. The magnitude of the dashpot is of the order of $\xi_{ac} \sim (kr_c)\kappa_S/\omega$, where k is the wave number of sound and r_c is the contact radius [24, 27].

3 Nonlinear Mechanics and Memory Effects

The standard model for analyzing QCM data is based on linear mechanics. All forces and stresses are assumed to be proportional to displacement or speed. Such a linear behavior is a prerequisite for equivalent circuits to apply. Nonlinear behavior, generally speaking, is often found in contact mechanics because of the sharp peaks in the stress distribution.

Importantly, the analysis of QCM data is not limited to situations, where stress and strain at the crystal surface are linearly related. In the presence of nonlinear interactions, the movement of the crystal becomes slightly anharmonic, meaning that it weakly deviates from a pure cosine. It is essential that the deviation from the purely harmonic motion is small. The two-timing approximation used below only holds for weakly nonlinear oscillators. However, since the perturbation of the crystal by the sample is small in any case, the nonlinear term in the dynamical equations governing the crystal's response are always small, as well. They are by far outweighted by the strong, linear stress-strain relation intrinsic to the crystal, even if the interaction between the crystal surface and the sample is strongly nonlinear. Assume that the crystal is in contact with a tip, which undergoes a transition from stick to slip: This would usually be considered a complicated situation. The interaction is so strongly nonlinear that the trajectory of the tip is highly hysteretic. Still: the tip only weakly perturbs the motion of the crystal and the analysis described below therefore holds.

The following section describes the use of the two-timing approximation for the analysis of QCM data. The same formalism is also used in the field of non-contact atomic force microscopy [28, 29]. In the latter context, the tip–sample interaction perturbs the oscillation of the cantilever. As long as the tip–sample force is weak compared to the force needed to bend the cantilever, the interaction potential can be reconstructed from the frequency of the cantilever as a function of amplitude and mean vertical distance.

The behavior of weakly nonlinear oscillators is discussed in the textbooks [30]. For a small external force $F(t)$, the two-timing approximation holds. The motion of the crystal is almost sinusoidal and the consequences of the external force are captured by a slowly varying amplitude $a(t)$ and a slowly varying phase $\Phi(t)$:

$$u(t) = a(t)\cos\left(\omega_0 t + \Phi(t)\right) . \tag{17}$$

$u(t)$ is the lateral displacement of the crystal surface and ω_0 is the resonance frequency of the unperturbed oscillator. The shift in bandwidth, $\Delta\Gamma$, is proportional to the time derivative of the amplitude, whereas the frequency shift, Δf, is proportional to the time derivative of the phase [31, 32]:

$$2\pi\Delta\Gamma = -\frac{1}{a}\frac{\mathrm{d}a}{\mathrm{d}t}$$

$$2\pi\Delta f = \frac{\mathrm{d}\Phi}{\mathrm{d}t} . \tag{18}$$

Here, the time increment $\mathrm{d}t$ is meant to be larger than the period of oscillation. This is the essence of the two-timing approximation. With regard to the details of the two-timing approximation, the reader is referred to [32]. The outcome of the calculation is [31, 32]:

$$\frac{\Delta f}{f_\mathrm{f}} = \frac{2}{a}\frac{1}{\pi A Z_\mathrm{q}}\frac{1}{\omega}\left\langle F(t)\cos(\omega t)\right\rangle \tag{19}$$

and

$$\frac{\Delta\Gamma}{f_\mathrm{f}} = \frac{2}{a}\frac{1}{\pi A Z_\mathrm{q}}\frac{1}{\omega}\left\langle F(t)\sin(\omega t)\right\rangle . \tag{20}$$

The angular brackets denote the average over an entire period of oscillation. The parameter ω is the frequency of the loaded oscillator (as opposed to ω_0). The difference between ω and ω_0 is small.

Note that the quantities in angular brackets are the exact same weighted averages which a lock-in amplifier (referenced to ω) would produce. Although the angular brackets look clumsy at first sight, they represent quantities which are very familiar to the experimentalist. They are the in-phase and the out-of-phase components of the force.

Equation 20 can be made plausible by noting that the term $\langle F(t)\sin(\omega t)\rangle$ is proportional to the energy dissipated per cycle:

$$\left\langle F(t)\sin(\omega t)\right\rangle = \frac{1}{a\omega_a}\frac{1}{T_\mathrm{p}}\int_0^{T_\mathrm{p}} F(t)\frac{\mathrm{d}u(t)}{\mathrm{d}t}\,\mathrm{d}t = \frac{1}{2\pi a}\oint F(u)\,\mathrm{d}u = \frac{1}{2\pi a}\Delta W , \tag{21}$$

where T_p is the period of oscillation and $\oint F(u)\,\mathrm{d}u = \Delta W$ is the area inside the hysteresis loop (see, for example, Fig. 4). The connection to the bandwidth is

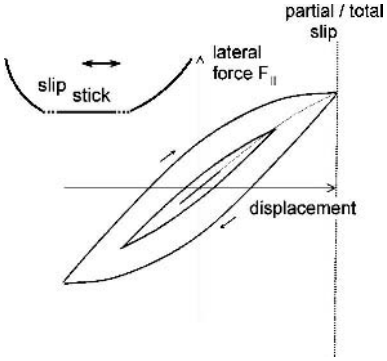

Fig. 4 Force–displacement relation as predicted by the Mindlin model. Since the central area, where the contact sticks, decreases with increasing tangential load, the force increases sub-linearly with displacement. The area under the hysteresis loop is the energy dissipated per cycle, ΔW

made by noting that the Q-factor of a resonance obeys the relation:

$$\Delta(Q^{-1}) = \frac{2\Delta\Gamma}{f} = \frac{\Delta W}{2\pi E_{\mathrm{osc}}} = \frac{\Delta W}{2\pi \frac{1}{2}\kappa_{\mathrm{p}} a^2}\,, \tag{22}$$

where $\Delta(Q^{-1})$ is the shift of the inverse Q-factor and $E_{\mathrm{osc}} = \kappa_{\mathrm{p}} a^2/2$ is the energy contained in the oscillation. Using the relation $(\kappa_{\mathrm{p}} m_{\mathrm{p}})^{1/2} = \kappa_{\mathrm{p}}/\omega = AZ_{\mathrm{q}} n\pi/2$ (Eq. 115 in Chap. 2), we find:

$$\begin{aligned}\frac{\Delta\Gamma}{f_{\mathrm{f}}} &= \frac{1}{f_{\mathrm{f}}}\frac{f}{2}\Delta(Q^{-1}) = n\frac{1}{2\pi\kappa_{\mathrm{p}} a^2}\Delta W \\ &= n\frac{1}{2\pi\kappa_{\mathrm{p}} a^2} 2\pi a\langle F(t)\sin(\omega t)\rangle \\ &= \frac{2}{AZ_{\mathrm{q}}\pi}\frac{1}{a}\frac{1}{\omega}\langle F(t)\sin(\omega t)\rangle\,,\end{aligned} \tag{23}$$

which reproduces Eq. 20. With regard to the frequency shift (Eq. 19), the argument is less intuitive and we leave it with the formal proof as given in [30].

When linear force laws hold, one has $F(t) = \kappa_{\mathrm{S}} u(t) + \xi_{\mathrm{S}}\dot{u}(t)$, which leads to:

$$\begin{aligned}\frac{\Delta f}{f_{\mathrm{f}}} &= \frac{1}{\pi Z_{\mathrm{q}}}\frac{1}{\omega}\frac{2}{A}\langle\kappa_{\mathrm{S}}\cos^2(\omega t)\rangle = \frac{1}{\pi Z_{\mathrm{q}}}\frac{1}{\omega}\frac{1}{A}\kappa_{\mathrm{S}} \\ \frac{\Delta\Gamma}{f_{\mathrm{f}}} &= \frac{1}{\pi Z_{\mathrm{q}}}\frac{1}{\omega}\frac{2}{A}\langle\omega\xi_{\mathrm{S}}\sin^2(\omega t)\rangle = \frac{1}{\pi Z_{\mathrm{q}}}\frac{1}{A}\xi_{\mathrm{S}}\,.\end{aligned} \tag{24}$$

Equations 19 and 20 then reduce to Eqs. 4 and 5. If memory effects are absent, a nonlinear stress–strain relation (quantified by a nonlinear spring constant $\kappa_{\mathrm{S}}(u)$) and a nonlinear stress–speed relation (quantified by a nonlinear drag

coefficient $\xi_S(\dot{u})$) can be explicitly reconstructed from the amplitude dependence of the Δf and $\Delta\Gamma$ [31, 32]. A unique solution is obtained. If, on the other hand, memory and hysteresis may not be neglected, no such explicit inversion of the equations is possible. Still, any assumption on the time-dependent force $F(t)$ can be inserted into Eqs. 19 and 20 in order to predict the frequency shift. The prediction can be compared with the experimentally determined frequency shift and the model can be refined until the prediction matches the experiment. By means of Eqs. 19 and 20, any given hypothesis about the force $F(t)$ (including stick-slip and memory effects) can be checked against the experiment.

4 Continuum Models

The circuits discussed in Sect. 2 contain discrete mechanical elements. They predict the sign, the n-dependence, and the relative magnitude of Δf and $\Delta\Gamma$, but they make no suggestion of how to assign a physical meaning to the model parameters, once they have been determined from experiment. Continuum models evidently are more complicated. On the other hand, they are not only more realistic, they also provide quantitative guidelines for the interpretation of experimentally derived parameters. Two situations have been analyzed, which are the sphere–plate contact and the sheet contact.

4.1 The Mindlin Model

The analysis of the sphere–plate contact under tangential oscillatory load goes back to Mindlin [12]. We refer the reader to [3] with regard to the derivation. Oscillatory tangential load is also discussed in the context for fretting wear [41, 42]. When a Hertzian sphere–plate contact is subjected to a tangential load, there is a stress concentration at the rim of the contact area. Within the continuum treatment, the stress goes to infinity at $r = r_c$, where r_c is the radius of contact. As a consequence, there is a ring-shaped area close to the rim of the contact, inside which the two surfaces slide against each other. The phenomenon is termed “partial slip”. As the stress increases, the sliding part of the contact zone increases in size, until it finally covers the entire contact. At this point, partial slip turns into gross slip.

If roughness plays a role, the Mindlin model does not apply. Still, the Mindlin model is a good example of a broader class of models of partial slip. Bureau et al. have proposed a quantitative extension of the microslip model accounting for multi-contact interfaces [34]. Partial slip also occurs in multi-asperity contacts because the microcontacts located at the rim are expected to rupture first. These contacts experience the largest lateral stress and the low-

est vertical load. While the details will certainly differ when comparing the Hertzian contact and the multi-asperity contact, the generic features should be similar.

Figure 4 shows the force–displacement relation for oscillatory tangential loading. The force–displacement curves bend downward because the part of the contact which sticks becomes smaller and smaller as the lateral force increases. The Hertzian contact is nonlinear under tangential load. (It is nonlinear under vertical load, as well.) The energy dissipated per cycle corresponds to the area inside the loop in Fig. 4. The dissipated energy does not depend on frequency. The Mindlin model describes a quasi-static motion. In particular, the energy dissipation entirely originates from the hysteretic behavior. Energy dissipated during sliding in the outer ring is neglected, which certainly is a shortcoming of the model.

For oscillatory loading, the lateral displacement, $u(t)$, is given by [3]:

$$u(t) = \frac{3\mu_S F_\perp}{8 r_c G_{\text{eff}}} \left[2\left(1 - \frac{F_{||,\max} - F_{||}(t)}{2\mu_S F_\perp}\right)^{\frac{2}{3}} - \left(1 - \frac{F_{\max}}{\mu_S F_\perp}\right)^{\frac{2}{3}} - 1 \right]$$

$$= \frac{3}{2}\lambda_S \left[2\left(1 - \frac{F_{||,\max} - F_{||}(t)}{2\mu_S F_\perp}\right)^{\frac{2}{3}} - \left(1 - \frac{F_{\max}}{\mu_S F_\perp}\right)^{\frac{2}{3}} - 1 \right], \tag{25}$$

where μ_S is the static friction coefficient, r_c is the radius of contact, $F_\perp$ is the vertiacl force, $F_{||}$ is the tangential force, and $F_{||,\max}$ is the maximum tangential force. $G_{\text{eff}} = 2 \times ((2 - \nu_1)/G_1 + (2 - \nu_2)/G_2)^{-1}$ is an effective modulus. G is the shear modulus, ν is Poisson's number, and the indices 1 and 2 label the contacting materials. We will show below that the quantity $4 r_c G_{\text{eff}}$ is the lateral spring constant of the contact in the low amplitude limit, $\kappa_{0,M}$. The characteristic length $\lambda_S = \mu_S F_\perp/(4 r_c G_{\text{eff}}) = \mu_S F_\perp/\kappa_{0,M}$, termed "partial slip length", was introduced for notational convenience. λ_S is defined in analogy to the elastic length $\lambda_e = F_\perp/\kappa$ (κ the lateral spring constant) used by the Paris group to describe multi-asperity contacts [35]. In macroscopic experiments, λ_e is a measure of roughness. λ_S differs from λ_e in that it contains the static friction coefficient μ_S as a prefactor. From the ratio of λ_S and λ_e, one obtains an estimate of the static friction coefficient.

Since the force across the contact only weakly perturbs the motion of the crystal surface, the displacement, $u(t)$, is mainly governed by the dynamics of the quartz crystal. $u(t)$ is sinusoidal with time, and the force $F(t)$ is a function of the displacement and the direction of motion. $F(t)$ can be calculated by inversion of Eq. 25 as:

$$\frac{F_{||}(t)}{\mu_S F_\perp} = \left[\frac{F_{||,\max}}{\mu_S F_\perp} - 2 + \frac{1}{\sqrt{2}} \left(1 + \frac{2u(t)}{3\lambda_S} + \left(1 - \frac{F_{||,\max}}{\mu_S F_\perp}\right)^{\frac{2}{3}} \right)^{\frac{3}{2}} \right]. \tag{26}$$

Inserting Eq. 26 into Eq. 24 and performing the integration leads to a prediction for Δf and $\Delta\Gamma$. In the small amplitude limit ($u(t) \ll \lambda_S$) one finds:

$$\frac{\Delta f}{f_f} \approx \frac{1}{AZ_q\pi}\frac{4r_cG_{eff}}{\omega}\left(1 - 0.20\frac{a}{\lambda_S}\right) = \frac{1}{AZ_q\pi}\frac{\kappa_{0,M}}{\omega}\left(1 - 0.20\frac{a}{\lambda_S}\right) \tag{27}$$

$$\frac{\Delta\Gamma}{f_f} \approx \frac{1}{AZ_q\pi}\frac{\kappa_{0,M}}{\omega}\frac{2}{9\pi}\frac{a}{\lambda_S}. \tag{28}$$

In the case of Eq. 27, the integration was carried out numerically. For the bandwidth (Eq. 28), analytical integration is possible because the integral is proportional to the area inside the hysteresis loop in Fig. 4 [3].

Comparing Eqs. 4 and 27, one sees that the term $4r_cG_{eff}$ can be identified with the spring constant in the small amplitude limit, $\kappa_{0,M}$. The dissipation is small, because the sliding portion of the contact is small. It is proportional to amplitude. This type of interfacial friction may therefore *not* be represented by a dashpot. However, there always is an additional source of dissipation given by radiation of sound into the sphere. This component can be modeled with a dashpot. The acoustic contribution to dissipation may mask interfacial friction at small amplitudes.

Figure 5 shows an example. A quartz crystal was covered with a monolayer of glass spheres (diameter $d = 200\,\mu m$) and exposed to humid air. In this case, the frequency shift and bandwidth were determined by ring-down [31, 32, 36]. The dependence of frequency and bandwidth on amplitude is substantial, indicative of a nonlinear interaction. From the slopes in the plots of Δf and $\Delta\Gamma$ vs a one infers a partial slip length λ_S of the order of

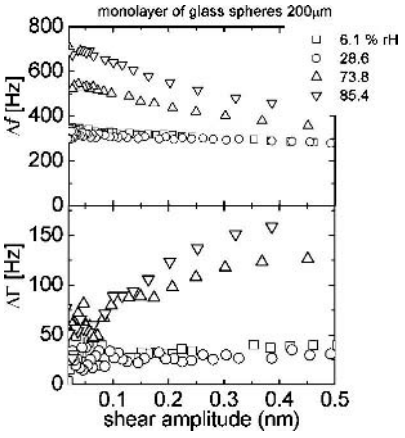

Fig. 5 Shift of frequency **a** and bandwidth **b** as a function of amplitude for a quartz plate covered with a monolayer of glass spheres ($d = 200\,\mu m$) at a various humidities. The data were acquired via ring-down [32]. From the slopes, one infers the partial slip length, λ_S and the coefficient of static friction, μ_s

a nanometer. The slips lengths derived from Δf and $\Delta \Gamma$ differ, indicating that the Mindlin model is not quantitatively applicable.

The sources of discrepancy are sliding friction, capillary interactions, and the fact that we have a multiasperity contact. Rolling (simultaneous release of contacts on one side and formation of new ones at the other) may also be part of the picture.

The elastic length $\lambda_e = F_\perp/\kappa_S$ is explicitly available: The spring constant, κ_S, can be derived from the frequency shift (Eqs. 4 and 27). The vertical force, $F_\perp$, is known from the weight of the spheres[2]. The static friction coefficient $\mu_S = \lambda_S/\lambda_e$ is significantly above one. High coefficients of static friction have also been found with colloidal probe experiments on quartz crystals (Gubaidullin and Johannsmann, in preparation). The reason for the increased static friction is subject to interpretation. Presumably, slip takes time: the MHz oscillation is just too fast for slip to set in [37]. This finding highlights, how much different the contact mechanics at high frequencies is from the corresponding behavior at low frequencies.

4.2 The Sheet-Contact Model

The Mindlin model describes the sphere–plate contact, assuming a contact radius much smaller than the radius of the sphere. The opposing limit, where the contact area is much larger than the wavelength of sound has been treated by the Shull group [38]. Such a geometry is established when a soft object like a hemisphere of a rubbery material touches the crystal. The JKR tester uses this arrangement [39]. The JKR model – underlying the JKR tester – is an extension of the Hertz model, accounting for a finite interfacial energy of the contacting materials. The interfacial interaction must be short-ranged. The model predicts the radius of contact as function of vertical load, stiffness of the material, and surface energy. The radius of contact usually is measured by imaging the contact from a above or below with a microscope. The JKR model and the JKR tester are frequently used in the study of polymer adhesion.

Clearly, combining the JKR tester with the QCM is attractive [38]. The material of interest is molded into the shape of a hemisphere and pushed against the top electrode of the QCM. From the shift in frequency shift and bandwidth one obtains the viscoelastic parameters of the material in the contact zone.

In passing, we note that this approach, in fact, is the only way to determine the viscoelastic parameters of rubbery polymers with the QCM. In principle, one might of course also coat the entire crystal with a thick layer of the respective material. If the thickness of the layer is larger than the penetration depth, the sample is acoustically semi-infinite. The Kanazawa equation

[2] This assumes that the external force is much larger than the force of adhesion.

applies and G' and G'' can be determined from Eq. 62 in Chap. 2 in this volume (using $G = \mathrm{i}\omega\eta$). Unfortunately, the QCM does not work well with semi-infinite media when the viscosity, η, is larger than about 50 cP. The shift of frequency and bandwidth in this case is too large. Most polymers exceed this limit. If, however, the contact area can be confined to a small spot in the center of the crystal, the bandwidth decreases accordingly and, the measurement becomes feasible.

Evidently, the contact established by the JKR-tester is laterally heterogeneous. Experiment shows that the finite contact area can reasonably well be accounted for by modifying the Kanazawa relation as:

$$\frac{\Delta f}{f_\mathrm{f}} = \frac{\mathrm{i}}{\pi Z_\mathrm{q}} K_\mathrm{A} \frac{A_\mathrm{c}}{A} Z_\mathrm{L}\,, \tag{29}$$

where A_c is the contact area and K_A is a "sensitivity factor" [38]. Equation 29 assumes a contact area much larger than the decay length of the shear wave. Also, energy trapping is assumed to be unaffected by the contact (which may be unrealistic in some situations).

The sensitivity factor, K_A, accounts for the non-trivial amplitude distribution over the area of the crystal. For small contact areas, K_A is about constant and equal to two [38]. Since the efficiency of energy trapping depends on overtone order, the parameter K_A depends on overtone order, as well. The K_A-factor can be determined by placing drops of water with known contact radius onto the center of the crystal. Equation 29 has been tested in that way and found to be a good approximation to the data for a large range of experimental conditions [38].

5 Concluding Remarks

The study of contact mechanics is just emerging as an application of the QCM. Clearly, there are limitations: the QCM probes the contacts at a frequency in the megaHertz range[3], it can only provide oscillatory excitation, and the amplitude of excitation is in the namometer range. Comparing the QCM to other devices of mechanical and micromechanical testing, there are following advantages and disadvantages:

- Due to the small amplitude of excitation, the contacts are not usually broken. The QCM is a device for non-destructive testing of interfacial contacts. The evolution of the contact strength with time, temperature, exposure to solvent vapor, or vertical pressure can be monitored without ever breaking a bond.

[3] Analogous studies can be done with torsional resonators in the kHz range. These have a lower sensitivity, but can bridge the frequency gap.

- Because the frequency is so high, inertia comes into play rather strongly. Balancing the force of interest (such as the force transmitted through the sphere–plate contact) against the force of inertia (holding the sphere in place), one gets around the often cumbersome problem of calibrating springs. In low frequency measurements, for example performed with the atomic force microscope, determination of the spring constant is a steady practical challenge. In a way, the situation is reminiscent of astronomy a few hundred years ago, where the force of gravity was analyzed based on a measurement of the orbital frequency of the planets (which admittedly is in a vastly different range).
- It is not true that the QCM is blind to nonlinear interactions. The QCM measures a peculiarly weighted average of the force, but it certainly can access nonlinear phenomena via the amplitude dependence of Δf and $\Delta \Gamma$.
- The QCM probes elastic and dissipative interactions at high frequencies. How relevant these high-frequency interactions are for real world devices, needs to be seen. We know today that things are much different at the MHz scale. We also know that fast processes are important in contact mechanics. Typical phenomena, where high-frequency events are crucial, are the sudden impact of a slider onto a substrate or the advancement of a crack tip in fracture events. At this point, the contact mechanics experiments with the QCM are part of fundamental research, but that may change.

Acknowledgements The author is indebted to Dr. Binyang Du for numerous fruitful discussions and making results available previous to publication.

References

1. Dowsan D (1998) History of tribology. Professional Engineering Publishing
2. Hertz H (1881) J Reine und Angew Mathem 92:156
3. Johnson KL (1989) Contact mechanics. Cambridge, NY
4. Persson BNJ (1998) Sliding friction. Springer, Berlin Heidelberg New York
5. Müser M, Urbakh M, Robbins MO (2003) Adv Chem Phys 126:187
6. Bushan B (ed) (1995) Handbook of Micro/nano tribology, CRC, Boca Raton
7. McClelland GM (1989) In: Grunze M, Kreuzer HJ (eds.) Adhesion and friction. Springer Series in Surface Science 17:1
8. Meyer E, Overney RM, Frommer J (1995) In: Bushan B (ed.) Handbook of micro/nano tribology. CRC, p 223
9. Tshiprut Z, Filippov, AE Urbakh, M (2005) Phys Rev Lett 95:016101
10. Homola AM, Israelachvili JN, Lee ML, McGuiggan PM (1989) J Tribolog 111:675
11. Homola AM, Israelachvili JN, McGuiggan PM, Lee ML (1990) Wear 136:65
12. Kumacheva E (1998) Progr in Surf Sci 58:75
13. Bowden FP, Tabor D (1967) Friction and lubrication. Methuen, London
14. Baumberger T, Heslot F, Perrin B (1994) Nature 367:544
15. Duran J (1999) Sands, powders, and grains. Springer, Berlin Heidelberg New York
16. Herminghaus S (2005) Adv Phys 54:221

17. Scherge M, Schaefer JA (1998) Tribolog Lett 4:37
18. Dybwad GL (1985) J Appl Phys 58:2789
19. Krim J, Solina DH, Chiarello R (1991) Phys Rev Lett 66:181
20. Mak C, Krim J (1998) Phys Rev B 58:5157
21. Bruschi L, Carlin A, Mistura G (2001) Phys Rev Lett 88:46105
22. König AM, Düwel M, Du B, Kunze M, Johannsmann D (2006) Langmuir 22:229
23. Laschitsch A, Johannsmann D (1999) J Appl Phys 85:3759
24. Watts ET, Krim J, Widom A (1990) Phys Rev B 41:3466
25. D'Amour JN, Stålgren JJR, Kanazawa KK, Frank CW, Rodahl M, Johannsmann D (2006) Phys Rev Lett 96:058301
26. Bocquet L, Charlaix E, Ciliberto S, Crassous J (1998) Nature 396:735
27. Berg S, Johannsmann D, Ruths M (2002) J Appl Phys 92:6905
28. Giessibl FJ (2001) Appl Phys Lett 78:123
29. Hölscher H, Schwarz UD, Wiesendanger R (1999) Appl Surf Sci 140:344
30. Strogatz S (1996) Nonlinear dynamics and chaos, chap 7.6. Addison-Wesley
31. Berg S, Prellberg T, Johannsmann D (2003) Rev Sci Instr 74:118
32. Berg S, Johannsmann D (2003) Phys Rev Lett 91:145505
33. Mindlin RD, Deresiewicz H (1953) J Appl Mech 20:327
34. Bureau L, Caroli C, Baumberger T (2003) Proc Royal Soc London A 459:2787
35. Berthoud P, Baumberger T (1998) Proc Royal Soc London A 454:1615
36. Rodahl M, Kasemo B (1996) Rev Sci Instr 67:3238
37. Maier S, Sang Y, Filleter T, Grant M, Bennewitz B, Gnecco E, Meyer E (2005) Phys Rev B 72:245418
38. Flanigan CM, Desai M, Shull KR (2000) Langmuir 16:9825
39. Shull KR (2002) Mat Sci Engin R 36:1
40. Zhang QL, Lec RM, Pourrezaei K (2006) IEEE TRANSACTIONS ON ULTRASONIC FERROELECTRICS AND FREQUENCY CONTROL 53(1):167–174
41. Szolwinski MP, Farris TN (1996) Wear 198:93
42. Varenberg M, Etsion I, Altus E (2005) Tribology Letters 19:263